Control of a Pneumatic Orthosis for Upper Extremity Stroke Rehabilitation

Eric T. Wolbrecht, John Leavitt, David J. Reinkensmeyer, and James E. Bobrow

Abstract— A key challenge in rehabilitation robotics is the development of a lightweight, large force, high degrees-of-freedom device that can assist in functional rehabilitation of the arm. Pneumatic actuators can potentially help meet this challenge because of their high power-to-weight ratio. They are currently not widely used for rehabilitation robotics because they are difficult to control. This paper describes the control development of a pneumatically actuated, upper extremity orthosis for rehabilitation after stroke. To provide the sensing needed for good pneumatic control, position and velocity of the robot are estimated by a unique implementation of a Kalman filter using MEMS accelerometers. To compensate for the nonlinear behavior of the pneumatic servovalves, force control is achieved using a new method for air flow mapping using experimentally measured data in a least-squares regression. To help patients move with an inherently compliant robot, a high level controller that assists only as needed in reaching exercises is developed. This high level controller differs from traditional trajectory-based, position controllers, allowing free voluntary movements toward a target while resisting movements away from the target. When the target cannot be reached voluntarily, the controller slowly builds up force, pushing the arm toward the target. As each target position is reached, the controller builds an internal model of the subject's capability, learning the forces necessary to complete movements. Preliminary testing performed on a non-disabled subject demonstrated the ability of the orthosis to complete reaching movements with graded assistance and to adapt to the effort level of the subject. Thus, the orthosis is a promising tool for upper extremity rehabilitation after stroke.

I. INTRODUCTION

APPROXIMATELY 700,000 people experience upper extremity movement impairment following a stroke in the U.S. each year [1]. Movement deficits are typically treated with intensive hands-on rehabilitation therapy. This is expensive and labor intensive, and therefore patients receive limited amounts of this therapy. To address this problem, several research groups have developed robotic devices for automating repetitive aspects of hands-on therapy following stroke (for reviews see [2]-[4]).

Initial clinical results with these devices have been promising. However, there is a general consensus that more sophisticated robotic devices would likely bring better clinical results. Of particular interest is the development of a device that can safely assist in fully naturalistic arm movements, and apply a large range of forces with good dynamic bandwidth. Such a device could implement a wide range of therapeutic interactions and movement exercises.

Pneumatic actuators can potentially help meet the challenge of lightweight, large force robots because they have a large power-to-weight ratio. Pneumatic actuators are also inherently compliant, providing a layer of safety. They have not been widely used for robotic rehabilitation primarily because they are difficult to control.

This paper describes the control development of a four degrees-of-freedom (DOF) pneumatically actuated orthosis, named Pneu-WREX, which can assist in naturalistic arm movements. The design allows for adjustment of upper arm length, forearm length, and shoulder position to fit a large range of subjects. Pneu-WREX is a modified version of a passive, anti-gravity arm support that uses elastic bands to relieve the weight of the user's arm (Fig. 1)[5]. As described in [6] pneumatic actuators were incorporated into WREX, producing the robotic device Pneu-WREX. The elastic counterbalance system was retained in Pneu-WREX so that the device will not fall when power is shut-off, and also because it expands the usable force range of the pneumatic actuators, since they do not have to overcome the weight of the orthosis. In the home position (right picture in Fig. 1 below) Pneu-WREX is able to produce 45, 55, and 70 N in the x (to the right), y (out from the body), and z (up) directions, respectively. Pneu-WREX is particularly strong along the $x = y$ axis, achieving forces in excess of 220 N.

E. T. Wolbrecht is with the Mechanical and Aerospace Engineering Department, University of California, Irvine, Irvine CA 92697 USA (phone: 949-824-8051; fax: 949-824-8585; e-mail: ewolbrecht@yahoo.com).

J. Leavitt is with the Mechanical and Aerospace Engineering Department, University of California, Irvine, Irvine CA 92697 USA (e-mail: leavittj@uci.edu).

D. J. Reinkensmeyer is with the Mechanical and Aerospace Engineering Department, University of California, Irvine, Irvine CA 92697 USA (e-mail: dreinken@ uci.edu).

J. E. Bobrow is with the Mechanical and Aerospace Engineering Department, University of California, Irvine, Irvine CA 92697 USA (e-mail: jebobrow@uci.edu).
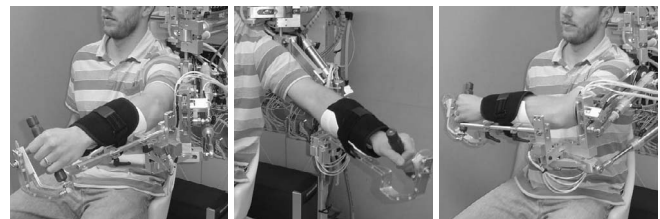
Fig. 1. Pneu-WREX. The device has four degrees-of-freedom (DOFs) corresponding to forward/backward clavicle rotation, shoulder flexion/extension, shoulder horizontal abduction/adduction, and elbow flexion/extension. Within these DOFs, the device allows nearly the full range of natural human arm motion.

Pneu-WREX has redundant potentiometers for position measurement. This configuration improves safety, eliminates the need for homing, and is inexpensive. However, discrete differentiation of a potentiometer signal produces a severely noisy velocity signal. As a unique solution to this problem, MEMS accelerometers are used as sensors in a Kalman filter to estimate the position and velocity of the end-effecter.

A hierarchical strategy was implemented for the control of Pneu-WREX, as documented in the literature by [7] and others. Cylinder chamber force control is achieved through feedback linearization, similar to [7] and [8]. To achieve good force control, the controller for Pneu-WREX uses a new method to linearize the air flow characteristics of the servovalve based on experimental data.

A previous paper provides a detailed description of the mechanical design of Pneu-WREX [6]. The high level controller described here uses the kinematics and Jacobian transformations developed in [6] as a starting point for task space control. A novel controller for rehabilitation therapy is presented that allows free movements toward a target position, without applying any forces initially. To achieve this, a controller with three primary parts was developed. The first part of the control scheme is a shrinking sphere centered at the target position. As the arm moves toward the target, the sphere shrinks. Movement away from the target is resisted by a standard PD force control law. The second part of the control scheme is an integral term that determines the static forces necessary to hold the arm at the target position. These static forces are stored into a lookup table, which acts as a sort of adaptive internal model of the patient's capabilities, and which is the third part of the control scheme. As the forces at different points are learned, data in the lookup table are used as the feedforward term in the controller. This technique compensates for the inherent compliance of the pneumatic actuators, which precludes the use of high-gain feedback control for accurate positioning of the patient's arm. The net effect is that the controller learns the static force needed to assist each patient at each workspace location, while maintaining an overall compliant, "human-like" feel to the assistance.

This paper first describes the safety features of Pneu-WREX, followed by a description of the Kalman filtering used for state estimation and control. Then it describes the low level force controller and high level controller for patient interaction. Finally, we present preliminary reaching tests with a non-disabled subject.

II. SAFETY

The design of Pneu-WREX has several inherent safety features, including:

1) Range of motion limits. Hard stops limit the range of motion to be less than that of the human arm, preventing the orthosis from forcing the arm into unnatural orientations.

2) Pneumatic limits. Pneu-WREX's strength is limited by supply pressure, and flow restrictions in the plumbing limit the rate of change in the force produced by the cylinders.

3) Pneumatic compliance. A pneumatic system can provide large forces but is still inherently compliant.

4) Upper arm spring mechanism. A four-bar spring mechanism provides counterbalance, keeping the orthosis from dropping in case of a loss of air pressure.

In addition, Pneu-WREX has several control safety systems, including:

1) Redundant position sensors. Each degree of freedom is measured by a linear potentiometer in the cylinders (Bimba PFC) and rotary position sensor (Midori CP-2FB).

2) Pneumatic exhaust system. A pneumatically piloted valve is plumbed between each cylinder chamber and its corresponding servovalve (Festo MPYE-5-1/8-LF-010-B). These valves exhaust the cylinders when the air supply is exhausted by the main solenoid valve.

3) Safety circuit. The main solenoid valve, which is normally closed when power is not supplied, is controlled by a safety circuit. This allows the system to be exhausted if the controller software detects a fault, if the control computer stops running, or if a safety stop switch is pressed.

4) Software fault detection. There are several software fault checks, including: low chamber pressure (using Honeywell ASCX100AN sensors), low supply pressure, desired chamber pressure, maximum velocity, and a redundant position check.

III. STATE ESTIMATION

In order to improve the position and velocity signals used for the control of Pneu-WREX, two 2-axis MEMS accelerometers (Analog Devices ADXL320EB) were installed on the end-effecter of the orthosis. Using the accelerometer measurements and the forward kinematics of the position sensors, a novel Kalman filter was designed to estimate the position and velocity of the end-effecter, similar to [9]. Using the spatial Jacobians developed in [6] the end-effector velocities are mapped back to both joint and cylinder velocities.

A. Estimator Design

With the accelerometers properly oriented the task space accelerations of the end-effector ($\ddot{x}$, $\ddot{y}$, $\ddot{z}$, and $\ddot{\theta}_z$) can be determined. Combined with the forward kinematics developed in [6], the state space equations for the measurement system are (shown below for the x direction).

$$\begin{bmatrix} \dot{\delta} \\ \dot{x} \\ \ddot{x} \end{bmatrix} = \begin{bmatrix} 0 & 0 & 0 \\ 0 & 0 & 1 \\ -\alpha & 0 & 0 \end{bmatrix} \begin{bmatrix} \delta \\ x \\ \dot{x} \end{bmatrix} + \begin{bmatrix} 0 \\ 0 \\ \alpha \end{bmatrix} a_m + \begin{bmatrix} 1 & 0 \\ 0 & 0 \\ 0 & -\alpha \end{bmatrix} \begin{bmatrix} v_b \\ v_a \end{bmatrix}$$

$$x_m = \begin{bmatrix} 0 & 1 & 0 \end{bmatrix} \begin{bmatrix} \delta \\ x \\ \dot{x} \end{bmatrix} + v_e \tag{1}$$

where δ and α are the accelerometer offset and scaling constants, a_m is the voltage measurement from the

accelerometer, x_m is the position measurement from the potentiometer, and v_b, v_a, & v_e are measurement noise. This system has the standard form

$$\dot{s} = As + Ba_m + B_v v_a$$
$$x_m = Cs + v_e \qquad (2)$$

where $s = \begin{bmatrix} \delta & x & \dot{x} \end{bmatrix}^T$ and A, B, B_v, C defined above.

A state estimator for the system is defined as

$$\dot{\hat{s}} = A\hat{s} + K\left(x_m - C\hat{s}\right) + Ba_m \qquad (3)$$

where K is the estimator gain. The error of the state estimator is

$$e = s - \hat{s}. \qquad (4)$$

Substituting (2) and (3) into (4),

$$\dot{e} = (A - KC)e \qquad (5)$$

If K is selected so that the eigenvalues of $A - KC$ have negative real parts, then $e(t) \to 0$ as $t \to \infty$.

A ¼ Hz, 10 cm peak-to-peak sine wave in the x direction of task space was tracked to evaluate control using the state estimator as compared to discrete derivative based control. In the control without state estimation, the desired force was passed through a 2nd order low-pass Butterworth filter. Fig. 2 below shows unfiltered and state estimations during tracking. Fig. 3 shows desired force and valve command signal (for one chamber) during tracking.
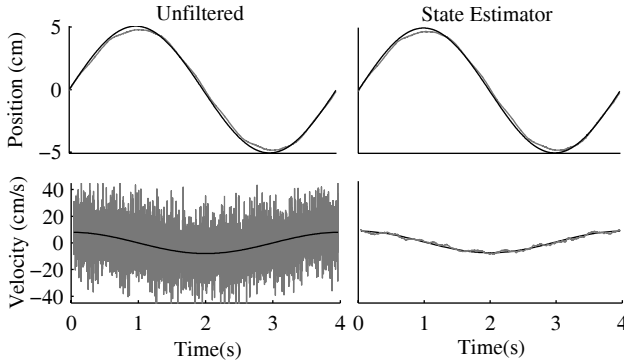

Fig. 2. Desired trajectory (black) and actual signals (grey) for unfiltered (left) and state estimates (right) while tracking a ¼ Hz sine wave.
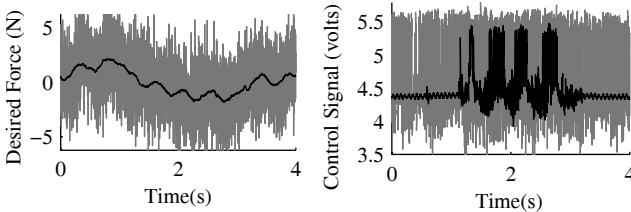

Fig. 3. Desired force and control signal using state estimates (black) and a low-pass 50 Hz Butterworth filter (grey).

The bottom right plot in Fig. 2 shows a substantial reduction in the noise associated with the velocity estimates. This improvement feeds through to the control signal as shown in Fig. 3, where the noise in the control signal is greatly reduced, resulting in less air consumption, reduced vibration, and quieter operation of the controller.

IV. PNEUMATIC FORCE CONTROL

A feedback linearizing, hierarchical strategy was implemented for the control of Pneu-WREX similar to that used in [7] and [8], but with two valves per cylinder instead of one. At the lowest level of the hierarchy is the pneumatic force controller, which controls the force output of each pneumatic cylinder.

The use of two servovalves per cylinder to control the net force output [10] has several advantages over a one servovalve per cylinder solution. Most notably, it allows the independent control of each side of the cylinder. By keeping cylinder chamber pressure as low as possible, friction and air consumption are decreased (as in [10],[11]) and safety is increased.

Utilizing the control techniques described in the following sections, Pneu-WREX is able to achieve a 3.5 Hz bandwidth while track a 5 cm peak-to-peak sine wave in the x direction of task space. The endpoint stiffness and dampening of this controller was 3.3 N/cm and 0.14 N-s/cm, respectively.

A. Single Chamber Force Control

The modeling of air flow dynamics is well documented by [12], [7] and others. Following these references, the differential equation for force, f, in a chamber of volume v and piston area a is

$$\dot{f} = kRT\left(a/v\right)\dot{m} - k\left(\dot{v}/v\right)f \qquad (6)$$

where R is the universal gas constant, T is the air temperature, and k is the ratio of constant pressure specific heat of air to constant volume specific heat of air.

In general the mass flow rate, $\dot{m}$, is a nonlinear function of valve spool position u, supply pressure p_s, and the chamber pressure. For now the nonlinear effects of air flow through the servovalve are ignored and the simple model

$$\dot{m} = c_f u \qquad (7)$$

is used, where c_f is the coefficient of the servovalve.

We choose our feedback control to be

$$u = \left\{k_p\left(f - f_d\right) + k_d \dot{f}_d\right\}(v/a) + k_v p\dot{v} \qquad (8)$$

where f_d is the desired force in the chamber, and k_p, k_d and k_v are the control gains. By substituting (8) and (7) into (6), and choosing k_d and k_v correctly, a linear first order ODE for the closed loop system is obtained so that $f(t) \to f_d(t)$ as $t \to \infty$ for a smooth trajectory $f_d(t)$ when $k_p < 0$.

B. Net Force Output Control

Ignoring the friction of the piston, the net force output is

$$f = f_1 - f_2 - f_{atm} \qquad (9)$$

where $f_{1,2}$ are the base and rod side forces, respectively, and f_{atm} is the force due to atmospheric pressure on the rod. From the desired net force of the piston, f_d, the

desired forces for each chamber are set to

$$f_{1d}, f_{2d} = \begin{cases} f_0 + f_d, f_0 & f_d \geq 0 \\ f_0, f_0 + f_d & f_d < 0 \end{cases} \quad (10)$$

where f_0 is the nominal force for each chamber. The nominal force is set slightly above atmospheric pressure, keeping friction and air consumption low, while maintaining a reasonable pressure differential for exhaust flow.

C. Air Flow through the Servovalve

The simplified model (7) for the air flow through the servovalve has two main deficiencies. The first is the deadband effect. The deadband is a region around the midpoint of the valve where no air flows in or out. The second is the flow dynamics of air through the valve geometry which are highly nonlinear. Past work has modeled the mass flow of air through a servovalve as mass flow through a variable orifice [14], or a nozzle. This approach has been combined with dead band compensation [13]. Others have added detailed effective flow area calculations [8]. These methods typically define separate equations for choked and unchoked flow, based on a critical pressure. These theoretical flow equations have been shown to be only approximations of actual mass flow through a servovalve [7]. For the control of Pneu-WREX, the mass flow relationship for the Festo servovalve was determined experimentally.

Flow experiments have been performed in the past by [7], [11], and others. For our experiments, two servovalves were set up in series with a chamber in the middle. Air was supplied to the first servovalve at 690 kPa and exhaust flow was measured on the second servovalve using a Honeywell AWM720P1 mass air flow sensor. The control voltage, u, for each valve was varied independently, creating different chamber pressure and flow combinations. Chamber pressure, p_c, and mass air flow, $\dot{m}$, were measured for each steady state flow condition. The collected data characterizes both flow into a chamber (through the first valve) and flow out of a chamber (through the second valve). Fig. 4 below shows data collected from the first servovalve, representing flow into the chamber from one of the experiments.
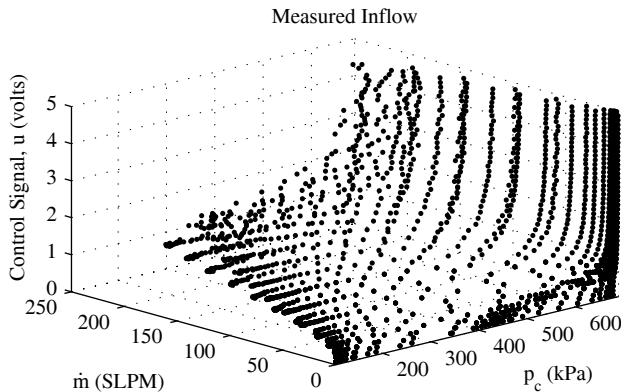

Fig. 4. Measured mass air flow into the chamber.

Attempts to fit the inflow data to the previously mentioned analytical functions resulted in a poor fit. Different functions were experimented with in order to find surfaces which better approximated the data. The best fitting function for inflow is

$$u = c_1 \dot{m}^2/(1 - p_c^{2.8})^{q_1} + c_2 \dot{m}^{1/5}/(1 - p_c^{2.8})^{q_2} + c_3 \dot{m}^{1/5} \quad (11)$$

where u is the valve command voltage, $\dot{m}$ is the measured mass flow, p_c is the chamber pressure, and c_{1-3} and q_{1-2} are the fitting constants.

To determine the constants in (11)

$$J = \left\| A(q)C - B \right\|^2 \quad (12)$$

was used as the cost function, where $C = [c_1, c_2, c_3]^T$ and $A(q)$ and B have i rows corresponding to each measured data point, with each row defined as

$$A_i = \left[\dot{m}_i^2/(1 - p_{c,i}^{2.8})^{q_1}, \dot{m}_i^{1/5}/(1 - p_{c,i}^{2.8})^{q_2}, \dot{m}_i^{1/5} \right]$$
$$B_i = \left[u_i \right] \quad (13)$$

The cost function was minimized in an iterative two step process. For the first step the q's were held constant and the backslash operator in Matlab was used to perform multiple linear regression to find the c's. In the second step the Matlab function *fminunc* was used for a nonlinear minimization of the q's while holding the c's at the values determined from the previous step. These two steps were repeated until the c's and the q's converged. These constants with (11) describe a surface relating the required valve voltage, u, to achieve a desired mass flow rate, $\dot{m}$, based on current chamber pressure, p_c. This surface is illustrated in Fig. 5 below.
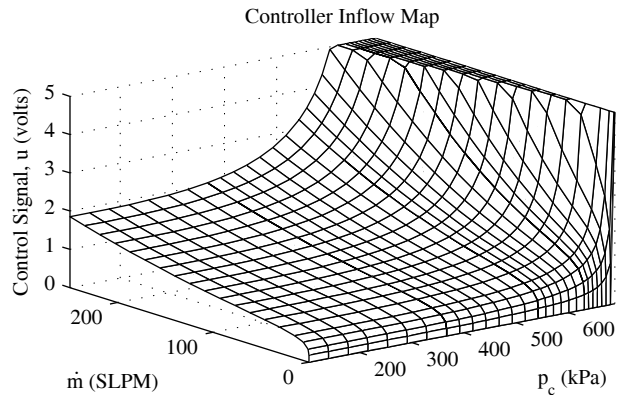

Fig. 5. Inflow map showing required valve spool voltage as a function of desired mass flow rate and chamber pressure. The map is truncated at 5 volts (the maximum of the valve).

Using different functions, the same process was repeated for the outflow data. This was necessary in order to account for the differences in the data. The force controller uses a different flow map for inflow (chamber pressurization) and outflow (chamber exhaust).

V. High Level Control for Patient Interaction

This section describes the high level controller for assisting in reaching movements. This controller determines force commands to the low-level force controller described in the previous section. Thus, the robot uses an outer loop that prescribes high level commands to the inner loop, which is the force control system. Jacobian matrices derived in [6] are used to transform cylinder forces to task space forces.

Pneumatically-actuated devices like Pneu-WREX are inherently compliant because of the compliance of air. This is acceptable for rehabilitation therapy applications because a compliant robot allows the patient to observe the outcome of changes in muscle force, thus encouraging voluntary participation, and does not rigidly hold the arm in an unsafe position. A pneumatic arm can be compared to a human therapist, who can apply large forces for assistance without being rigid. The high level controller described here can also apply large forces that help the patient move without being rigid.

The controller described here differs from standard position controllers in that initially it applies no force to the arm. Rather than specifying a trajectory, we specify a desired target point, applying forces only when progress toward the target is inadequate, as explained next.

A. Shrinking Sphere PD control

A three part high level controller for Pneu-WREX has been implemented. The first part of the controller is a shrinking sphere PD based controller. It is designed to assist in point to point reaching movements, a common rehabilitation exercise [15]. The applied force from the controller is

$$\vec{F}_{PD} = \begin{cases} -k_P\left(r - r_s\right)\vec{u} - k_D\dot{\vec{x}} & r > r_s \\ -k_D\dot{\vec{x}} & otherwise \end{cases} \quad (14)$$

where $\vec{F}_{PD}$ is the applied force vector , $r = \left\|\vec{x} - \vec{x}_t\right\|$ is the radius distance from the arm location $\vec{x}$ to the target point $\vec{x}_t$, r_s is the radius of the sphere, and $\vec{u}$ is a unit vector pointing from $\vec{x}$ from $\vec{x}_t$. The constants k_P and k_D are the proportional and derivative gains, respectively. The sphere radius, r_s, is initialized as the initial radius distance r. From that time forward r_s is equal to

$$r_s\left(t + \Delta t\right) = \min\left(r_s\left(t\right)d_s\left(1 - e^{(-gt)}\right), r\left(t\right)\right) \quad (15)$$

where $0 < d_s < 1$ is the decay rate of the sphere, t is the time from the last target change, and Δt is the discrete sample time. This equation sets $r_s = r$ as $\vec{x}$ approaches $\vec{x}_t$, and decays r_s when no movement is made toward the target. The term $1 - e^{-gt^2}$ gives the patient a chance to reach voluntarily before r_s begins to decay, with g used to adjust this voluntary reach time.

This control law allows initial un-resisted movement towards the target. When movement is made towards the target the sphere shrinks and movement away from the target is resisted in a proportional manner. Similar concepts have been explored by [16],[17].

B. Force Integrator with Forgetting

The second part of the high level control is the integral term with forgetting, similar to [18]

$$\vec{F}_I\left(t + \Delta t\right) = \vec{F}_I\left(t\right)f_I - k_I\Delta t\left(r\left(t\right) - r_s\left(t\right)\right)\vec{u} \quad (16)$$

where $\vec{F}_I$ is the applied force vector, and k_I is the integral gain. The integral forgetting factor, $0 < f_I < 1$, reduces $\vec{F}_I$ when $r - r_s$ is small. This encourages the subject to provide as much force as possible. This integral term slowly generates force pulling the arm toward the target when $r > r_s$. Thus, the robot eventually accurately positions the arm even though the robot is inherently compliant.

Once the target position is reached, the required forces are stored in the lookup table. Then a new desired position is specified, the sphere radius is reset, and the reach time is set to zero.

C. Lookup Table: Forming a Model of the Patient's Ability

The final part of the high level controller is a lookup table for storing the forces required to hold the arm at various targets points. The lookup table applies force to the arm as a function of arm position. These forces compensate for the arm weight and muscle tone that a patient is unable to overcome by effort alone.

The lookup table applies forces according to

$$\vec{F}_T = \vec{F}_{LWA}f_T \quad (17)$$

where $\vec{F}_T$ is the applied force from the lookup table and $\vec{F}_{LWA}$ is a locally weighted average of the stored forces based on the Gaussian kernel. The table forgetting factor, $0 < f_T < 1$, allows the subject to reach to a target with less assistance than the previous reach to the same target.

Once at the new target, the lookup table will store the new total force of the three part controller. This allows the lookup table to adjust as the patient needs more or less assistance.

D. High Level Controller Testing

Two sets of reaching tests were performed on the left arm of a non-disabled, 33-year-old, male subject. In the first set of reaching tests, the subject repeated the same point to point reaching motion three times. The subject started with the hand in front of the abdomen. He reached up and out to the left of the body. Fig. 6 below shows the reaching motion in the frontal plane (i.e. the $x - z$ plane, where positive z is up and positive x is right, and the origin of this coordinate system is the center of the left shoulder). Forces are shown as vectors in these figures at 0.25 second intervals.
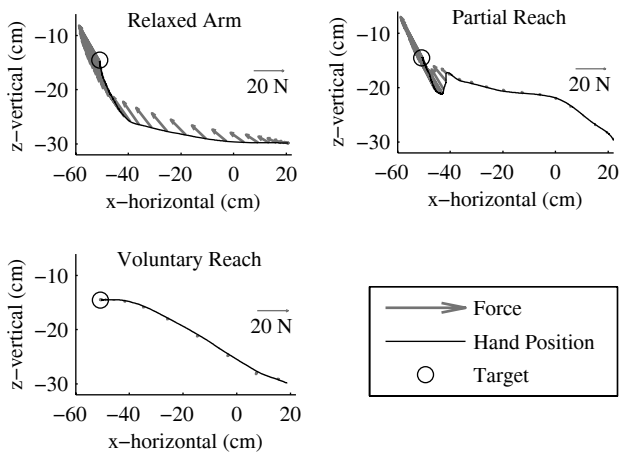
Fig. 6. High level controller response for point to point reaching. When the subject reached voluntarily to the target (voluntary reach and first half of partial reach), the robot did not apply force. When the subject relaxed (relaxed arm, and second half of partial reach), the robot supported the arm and slowly moved the arm to the target
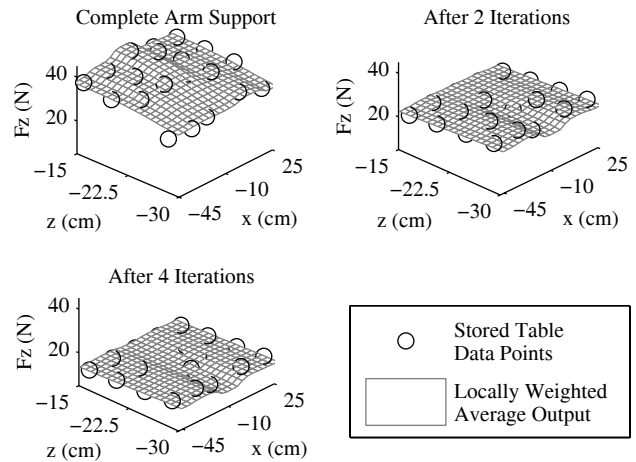
.

Fig. 7. High level controller testing. The subject first relaxed his arm while the controller completed 24 reaches (top left) Next, the subject reached voluntarily to the same 24 targets for 4 iterations (top right and bottom left). Circles are points stored in the lookup table, and the surfaces are the output from the locally weighted average.

In the first reach, the subject was instructed to relax the arm. The force integrator slowly generated force as the sphere shrunk, moving the subject's arm to the target.

For the second reach, the subject was instructed to reach halfway to the target and then relax his arm (top right Fig. 6). The orthosis applied small forces as the subject moved his arm voluntarily toward the target, and then larger forces as the subject relaxed his arm. The dip in trajectory was stopped by the shrinking sphere force, allowing the force integrator to build up force and move the arm to the target.

In the third test, the subject was instructed to reach all the way to the target (bottom left Fig. 6). Here the orthosis applied only small forces during the entire voluntary reach.

For the second set of tests, the subject made reaches toward 24 targets distributed across a frontal plane, returning to a central target between each reach. In the first test, the subject was instructed to relax the arm, allowing the controller to complete all 24 reaches. The data in the lookup table was stored and used as the initial lookup table for the second test. In the second test, the subject was instructed to perform 4 iterations of voluntary reaching toward the same 24 targets.

The top left of Fig. 7 shows the stored lookup table points and output from the locally weighted average after the controller completed the reaches while the subject relaxed his arm. This output is the required force to hold the weight of the subject's arm at each target. The top right and bottom left of Fig. 7 show the same output after the subject performed voluntary reaching toward the same targets after 2 and 4 iterations, respectively. This demonstrates the ability of the lookup table to reduce output as the subject provides more effort. In this way, the controller is able to adapt to the ability of the subject.

VI. DISCUSSION/CONCLUSION

These results demonstrate the feasibility of using pneumatic actuation for a robotic therapy device. Pneumatic actuators have the advantage of a large power-to-weight ratio. Thus, the device described here can lift a large human arm, and position it across a wide workspace, a common goal in rehabilitation exercise. The device currently has four DOFs, allowing a reasonable range of functional movements but not fully naturalistic movement. Adding more degrees-of-freedom (e.g. shoulder internal/external rotation) is feasible because pneumatic actuators are relatively lightweight.

A deterrent to using pneumatic actuators is that they are difficult to control relative to electric motors. This paper shows how low-cost sensors and a Kalman filter can provide the effective sensing necessary for pneumatic control. This paper also provides an experimentally-identified model of a low-cost servovalve that allows the robot to achieve desired force control.

A novel high level controller was developed that assists the user of the device in moving the arm to a desired target, but only as needed. The controller learns an internal model of the static forces required to hold the user's arm at different workspace locations, allowing accurate positioning while maintaining a compliant "feel" to the assistance.

A possible disadvantage of the pneumatic approach used here is that the robot cannot be made rigid, and the robot cannot be made to have a very high force or position tracking bandwidth. However, the stiffness and bandwidth achieved are similar to that of the human arm itself. Thus, if the arm of a human therapist is sufficient to produce optimal rehabilitation results, then a pneumatic device such as the one describe here should also be sufficient for optimal rehabilitation results, given appropriate high level control strategies.

REFERENCES

[1]   A. H. Association, "Heart Disease and Stroke Statistics – 2005 Update," Dallas, Texas.: *American Heart Association*, 2005.

[2]   N. Hogan and H. Krebs, "Interactive robots for neuro-rehabilitation," *Restorative Neurology and Neuroscienc*e, vol. 22, pp. 349-358, 2004.

[3]   D. Reinkensmeyer, J. Emken, and S. Cramer, "Robotics, motor learning, and neurologic recovery," *Annual Review of Biomedical Engineering*, vol. 6, pp. 497-525, 2004.

[4]   R. Riener, T. Nef, and G. Colombo, "Robot-aided neurorehabilitation of the upper extremities," *Medical & Biological Engineering & Computing t*, vol 43, pp. 2-10, 2005.

[5]   T. Rahman, W. Sample, and R. Seliktar, "Design and testing of WREX," *presented at The Eighth International Conference of Rehabilitation Robotics*, Kaist, Daejeon, Korea, 2003.

[6]   R. J. Sanchez, et al, "A pneumatic robot for re-training arm movement after stroke: rationale and mechanical design," *Rehabilitation Robotics, 2005. ICORR 2005. 9th International Conference on* , vol., no.pp. 500- 504, 28 June-1 July 2005.

[7]   J. E. Bobrow and B. W. McDonell, "Modeling, identification, and control of a pneumatically actuated, force controllable robot," *IEEE Transactions on Robotics and Automation*, vol. 14, pp. 732-42, 1998.

[8]   E. Richer and Y. Hurmuzlu, "A high performance pneumatic force actuator system: part 1 – nonlinear mathematical model," *ASME Journal of Dynamic Systems, Measurement, and Control*, vol. 122, no. 3, pp. 416-425, 2000.

[9]   Leavitt, J., Sideris, A., Bobrow, J.E., "Bandwidth tilt measurement using low cost sensors," *American Control Conference, 2004. Proceedings of the 2004*, vol.3, no.pp. 2184- 2189 vol.3, 30 June-2 July 2004

[10] Al-Dakkan, K.A.; Goldfarb, M.; Barth, E.J., "Energy saving control for pneumatic servo systems," *Advanced Intelligent Mechatronics, 2003. AIM 2003. Proceedings. 2003 IEEE/ASME International Conference on*, vol.1, no.pp. 284- 289 vol.1, 20-24 July 2003.

[11] Granosik, G.; Borenstein, J., "Minimizing air consumption of pneumatic actuators in mobile robots," *Robotics and Automation, 2004. Proceedings. ICRA '04. 2004 IEEE International Conference on*, vol.4, no.pp. 3634- 3639 Vol.4, April 26-May 1, 2004.

[12] J. L. Shearer, "Study of pneumatic processes in the continuous control of motion with compressed air – i,ii," *Transactions of ASME*, pp. 233-242, February 1956.

[13] F. Xiang and J. Wikander, "Block-oriented approximate feedback linearization for control of pneumatic actuator system," *Control Engineering Practice*, 12(4):387-399, 2004.

[14] F. E. Sanville, "A new method of specifying the flow capacity of pneumatic fluid power valves," *Hydraulic Pneumatic Power*, 17(195), 1971.

[15] R. Sanchez, et al, "Monitoring functional arm movement for home-based therapy after stroke," *Engineering in Medicine and Biology Society, 2004. EMBC 2004. Conference Proceedings. 26th Annual International Conference of the*, vol.2, pp. 4787- 4790 Vol.7, 1-5 Sept. 2004.

[16] Buerger, S.P.; Palazzolo, J.J.; Krebs, H.I.; Hogan, N., "Rehabilitation robotics: adapting robot behavior to suit patient needs and abilities," *American Control Conference, 2004. Proceedings of the 2004* , vol.4, no.pp. 3239- 3244 vol.4, 30 June-2 July 2004.

[17] P. S. Lum, C. G. Burgar, P. C. Shor, M. Majmundar, and M. Van der Loos, "Robot-assisted movement training compared with conventional therapy techniques for the rehabilitation of upper-limb motor function after stroke," *Arch Phys Med Rehabil*, vol. 83, pp. 952-9, 2002.

[18] J. L. Emken, J. E. Bobrow, and D.J. Reinkensmeyer, "Robotic movement training as an optimization problem: designing a controller that assists only as needed," *Rehabilitation Robotics, 2005. ICORR 2005. 9th International Conference on*, Chicago, IL, pp. 307-312, 28 June-1 July 2005.